Ion Structure Near a Core-Shell Dielectric Nanoparticle

Manman Ma,[*] Zecheng Gan,[†] and Zhenli Xu[‡]

*School of Mathematical Sciences, Institute of Natural Sciences, and MoE Key Lab of Scientific and Engineering Computing,
Shanghai Jiao Tong University, Shanghai 200240, China*

A generalized image charge formulation is proposed for the Green's function of a core-shell dielectric nanoparticle for which theoretical and simulation investigations are rarely reported due to the difficulty of resolving the dielectric heterogeneity. Based on the formulation, an efficient and accurate algorithm is developed for calculating electrostatic polarization charges of mobile ions, allowing us to study related physical systems using the Monte Carlo algorithm. The computer simulations show that a fine-tuning of the shell thickness or the ion-interface correlation strength can greatly alter electric double-layer structures and capacitances, owing to the complicated interplay between dielectric boundary effects and ion-interface correlations.

Core-shell structured nanoparticles (NPs) refer to inner cores surrounded by outer materials as shells, with a total size between 1 and 100 nm. They have been utilized for numerous applications in physical chemistry, biomedical engineering [1], and energy storage devices [2,3]. In these applications, the core-shell NPs are often favored in comparison with classical homogeneous NPs, since various preferable physical properties can be achieved due to the core-shell architecture, such as extraordinary robustness [4], higher energy storage capability [5], and enhanced optical effects [6]. The core-shell structures have been found to play an important role in the NP's self-assembly, and thus is useful for synthesis of new materials [7]. In the field of electrochemical supercapacitors, excellent performance of core-shell structured dielectric nanomaterials has motivated many experiments [8–10] to widely investigate effects of different properties of core-shell NPs.

Dielectric properties are of great importance since dielectric constants for different materials can range in a large interval from 2–12 (e.g., organic polymers) to 100–10 000 (e.g., dielectric ceramics). These properties have attracted broad attention in vast applications, e.g., air-electrolyte interface and colloidal science [11,12], in addition to the field of electric double-layer (EDL) capacitors where high-dielectric metal electrodes are often used. In addition, the electronic polarization on surfaces plays an essential role for various electrode materials [13–15], for which particle simulations to account for charge fluctuations [16,17] on the electrode are computationally intensive. Dielectric effects for a single planar surface were well studied [18,19] since the image-charge method (ICM) can be easily employed. However, core-shell dielectric structures are not well understood in theory in spite of abundant experiments in literature [1,3,20]. The presence of multiple dielectric interfaces leads to a great challenge in the numerical approximation of ion-ion interactions, because a 3D Poisson's equation has to be solved in order to obtain polarization charges induced on the interfaces. Proper treatments for multilayered dielectric effects of spheres have rarely appeared in the literature since the last well-established theory for layered dielectric spheres derived by Lindell *et al.* [21]. Simulation techniques [12,22–25] have made great progress for heterogeneous dielectric media, but applications to the core-shell structure for a satisfactory accuracy remain challenging.

In this Letter, we first develop a generalized ICM for the Green's function in the use of Monte Carlo (MC) methods for simulating the ion structure around a core-shell dielectric NP, which can efficiently calculate the polarization contribution. Applying the ICM, we show that the self-energy profile of a single ion outside a core-shell NP can be qualitatively different from the dielectrically homogeneous case even for a thin shell thickness. The effect of polarization charges on ionic distributions and EDL capacitances is further explored through MC simulations which demonstrate that, by fine-tuning the shell thickness and the ion-interface correlation strength, the polarization charges can greatly alter EDL structures and capacitances of the system. As explained below, we attribute enhanced EDL capacitances to dielectric boundary attractions and strong correlations between ions in the electrolyte and partial charges on the interface.

The Green's function $G(\mathbf{r}, \mathbf{r}')$ for a medium composed of a dielectric core-shell NP of radius R and the solvent is described by the Poisson's equation,

$$-\nabla \cdot \eta(\mathbf{r})\nabla G(\mathbf{r}, \mathbf{r}') = 4\pi\delta(\mathbf{r} - \mathbf{r}'), \quad (1)$$

where $\eta(\mathbf{r}) = \varepsilon(\mathbf{r})/\varepsilon_w$ characterizes the relative dielectric function which is piecewise constant. Here, $\varepsilon(\mathbf{r})$ is material specific and ε_w is that of the solvent. Suppose the radius of the core and the thickness of the shell are $R_c = (1 - \theta)R$ and $R_s = \theta R$, respectively, then the value of η takes η_c within the core, η_s in the shell layer, and 1 in the solvent.
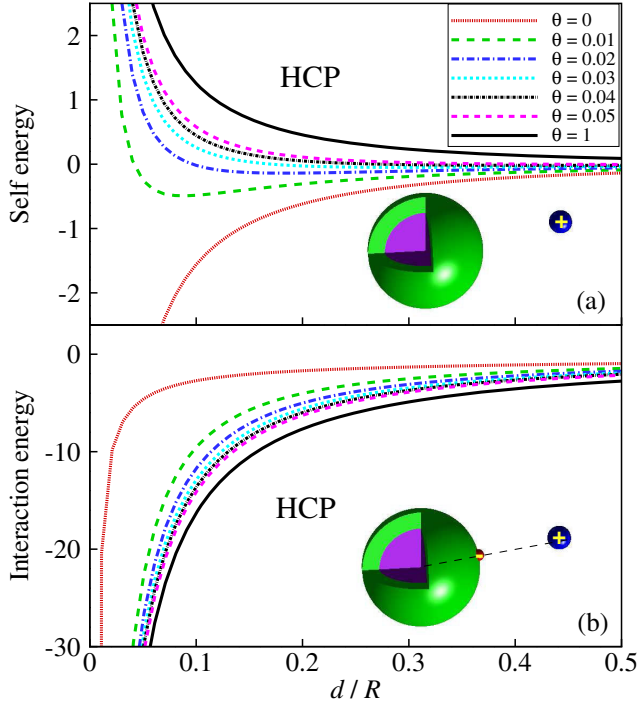
FIG. 1. Self-energy of a cation (a) and interaction energy between a cation and an interfacial anion (b) which are collinear with the NP center, in the presence of a HCP for different shell thicknesses. Energy unit $(\ell_B/R)k_BT$.

In the following discussion, we use two opposite combinations of dielectric constants: $(\eta_c, \eta_s) = (10, 0.1)$ for the dielectric high-core low-shell particle (HCP) and $(\eta_c, \eta_s) = (0.02, 10)$ for the dielectric low-core high-shell particle (LCP).

The dielectric effect due to the core-shell structure turns out to be physically interesting even when only a single ion is present. In Fig. 1(a), we plot the self-energy of a cation with valence $z = 1$ near a HCP for different shell thicknesses as a function of the distance of the source from the surface $d = r' - R$, where the self-energy is defined as $\frac{1}{2}z^2\ell_B G_{\text{pol}}(\mathbf{r}', \mathbf{r}')$, with G_{pol} given later in Eq. (2), and the coupling parameter $\ell_B = e^2/(4\pi\varepsilon_0\varepsilon_w k_B T)$ is the Bjerrum length of the solvent with the elementary charge e, the vacuum permittivity ε_0, the Boltzmann constant k_B, and temperature T. At short range from the surface, the qualitative change in self-energy profiles between $\theta = 0$ and 0.01 indicates a *discontinuous* transition from attraction into repulsion, which shows a clear dominance of the coated shell material over the core material even though the shell is very thin. This phenomenon can be understood from the asymptotics of G_{pol} as $d \ll R$ by using the Mellin transform. As θ increases from zero to a positive value, the leading asymptotics changes from an image point to an image dipole with an opposite sign (details shown in Supplemental Material [26]). When the ion is at a long distance from the surface, the ion-NP interaction turns *continuously* from attraction into repulsion with the
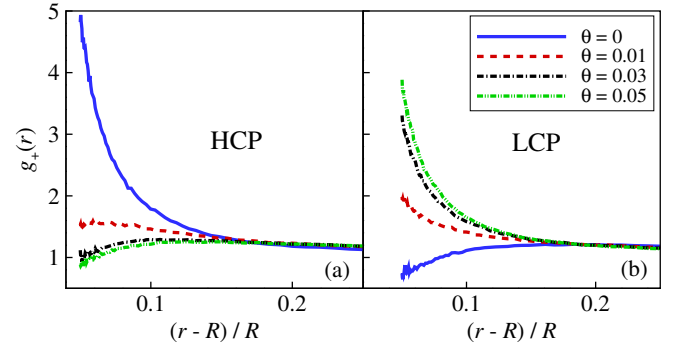
FIG. 2. With a given surface charge density $\sigma = -10e/(4\pi R^2)$ and correlation strength $\nu = 0.1$, RDFs of counterions versus dimensionless positions with different shell thicknesses are shown in (a) for the HCP and (b) for the LCP.

increase of θ, which is also in agreement with the asymptotic analysis [26]. At a certain thickness [in Fig. 1(a) when $\theta = 0.01$], the nonmonotonic behavior is observed, which is explained as the competition between the core attraction and shell repulsion. This competition could further influence the intrinsic EDL structure and related physical properties when the NP is immersed in an electrolyte (Fig. 2). The calculation of the interaction energy between two ions, a test ion and an interfacial ion, which are collinear with the center of the NP, also shows the great discrepancy for different shell thicknesses and stronger interactions for larger θ [see Fig. 1(b)]. This discrepancy will certainly modify the EDL structure and macroscopic properties of core-shell NP systems.

The Green's function Eq. (1) is solved by constructing a generalized image charge formula. To start, one solves the Green's function by the spherical harmonic expansion as $G(\mathbf{r}, \mathbf{r}') = 1/|\mathbf{r} - \mathbf{r}'| + G_{\text{pol}}(\mathbf{r}, \mathbf{r}')$, where the polarization contribution is

$$G_{\text{pol}}(\mathbf{r}, \mathbf{r}') = \frac{R}{r'}\sum_{n=0}^{\infty}\frac{r_K^n}{r^{n+1}}P_n(\cos\varphi)M(n), \qquad (2)$$

$$M(n) = S_0(n) + S_1(n), \qquad (3)$$

where $r_K = R^2/r'$ denotes the radial position of the Kelvin point along $\mathbf{r}'$, $P_n(\cdot)$ is a Legendre polynomial of order n, φ is the angle of $\mathbf{r}$ and $\mathbf{r}'$, and $S_0(n) = (1-\eta_s)n/[(1+\eta_s)n+1]$ is the regular solution for a NP with a uniform dielectric constant [28]. $S_1(n)$ takes into account the effect of dielectric nonuniformity, and thus is a function of η_s and η_c:

$$S_1(n) = -\frac{\frac{\eta_s n(2n+1)^2}{[(1+\eta_s)n+1][(\eta_c+\eta_s)n+\eta_s]}(1-\theta)^{2n+1}}{\frac{(1+\eta_s)n+1}{\eta_c-\eta_s} - \frac{(1-\eta_s)n(n+1)}{(\eta_c+\eta_s)n+\eta_s}(1-\theta)^{2n+1}}. \qquad (4)$$

Equation (2) has a slow convergence rate when a charge is close to the interface, and will not provide a rapid algorithm for the MC simulation of NP systems. To avoid the use of it, the image charge expression can be invoked by

introducing the Mellin transform, $M(n) = \int_0^1 N(t)t^{n-1}dt$, where the harmonic coefficient $M(n)$ is continued into a function over the complex plane and its inverse Mellin transform converts G_{pol} into an integral form. With $N(t)$ solved, the expression is

$$G_{pol} = \frac{R}{r'}\int_0^1 N(t)\sum_{n=0}^{\infty}\frac{r_K^n t^{n-1}}{r^{n+1}}P_n(\cos\varphi)dt$$
$$= \int_0^{r_K}dx\frac{\rho(x)}{|\mathbf{r}-\mathbf{x}|}, \qquad (5)$$

with a line charge density $\rho(x) = N(x/r_K)/(Rx/r_K)$. In the case of a NP with a uniform dielectric constant η, i.e., the limit of $S_1(n) = 0$ and $\eta \equiv \eta_s$, this transformation gives the well-known solution of the Neumann image principle [29,30],

$$G_{pol}^{S_1\to0} = \frac{1-\eta_s}{1+\eta_s}\frac{r_K}{R|\mathbf{r}-\mathbf{r}_K|}$$
$$-\frac{1-\eta_s}{(1+\eta_s)^2R}\int_0^{r_K}\frac{(x/r_K)^{-\eta_s/(1+\eta_s)}}{|\mathbf{r}-\mathbf{x}|}dx, \quad (6)$$

which removes the difficulty of the slow convergence of spherical harmonic series [Eq. (2)] by discretizing the line integral [31].

Unfortunately, no analytical inverse Mellin transformation for $S_1(n)$ is available. The Padé approximation is employed as $S_1(n) \approx \tilde{S}_1(P,n)$ and

$$\tilde{S}_1(P,n) = \alpha_0 + \sum_{i=0}^{P-1}p_i n^i \Big/ \left(n^P + \sum_{i=0}^{P-1}q_i n^i\right), \quad (7)$$

where constant coefficients α_0 and p_i, q_i ($i = 0, ..., P-1$) are then determined by the nonlinear least-squares method following the idea proposed in a multiscale model of electrolytes using the Poisson-Boltzmann equation [32]. A larger P corresponds to a higher accuracy in the Padé approximation. The inverse Mellin transform for rational polynomial $\tilde{S}_1(P,n)$ is obtained analytically, which gives an approximate image potential,

$$\tilde{G}_{pol} = \int_0^{r_K}dx\frac{\tilde{N}(x/r_K)/(Rx/r_K)}{|\mathbf{r}-\mathbf{x}|}, \qquad (8)$$

with $\tilde{N}(x/r_K)$ being an approximation of $N(x/r_K)$. The Green's function can now be well approximated by a summed contribution of the source charge and point image charges after applying numerical integration (e.g., Gauss-Legendre or Gauss-Radau) [31] to the line integral, $\tilde{G}(\mathbf{r},\mathbf{r}') = 1/|\mathbf{r}-\mathbf{r}'| + \sum_{m=1}^M \rho_m'/|\mathbf{r}-\mathbf{x}_m|$ with a small number M. The locations $\mathbf{x}_m$ and strengths ρ_m' of image point charges all explicitly depend on the source charge location $\mathbf{r}'$. In comparison with the direct calculation of the harmonic series Eq. (2), the ICM at the same level of accuracy can achieve the speed-up for $\sim$50 times, as

demonstrated in Supplemental Material [26]. Compared to grid-based methods such as the boundary element method, the ICM has natural merit since it avoids solving a linear algebraic system, which becomes increasingly ill conditioned when ions approach the interface.

With the ICM, we implement the standard canonical-ensemble MC algorithm for the primitive-model electrolyte within a Wigner-Seitz spherical cell [33], where a core-shell structured NP is located at the center. The ICM is used to calculate interactions between ions in the electrolyte, which depend on the position of the NP. We take a binary electrolyte with monovalent salt. The NP has a total surface charge $Q = \pm\nu e N_s$ modeled as N_s discrete point charges $\pm\nu e$ distributed on the surface, which are mobile and confined on the surface [34]. The Hamiltonian of the system is expressed as the sum of interactions among all ions and surface charges $z_i z_j \ell_B G(\mathbf{r}_i, \mathbf{r}_j)$ ($z_i = \pm\nu$ for surface charges), the self-energies of mobile ions $\frac{1}{2}z_i^2\ell_B G_{pol}(\mathbf{r}_i, \mathbf{r}_i)$, the hard-core repulsion energy among all ions and electrolyte boundaries, and the potential used to confine those discrete charges on the surface.

The above model describes a prototypical system of a dielectric core-shell NP immersed in electrolyte. The surface-charge model with discrete and mobile interfacial ions captures the strong coupling between surface charges and mobile ions, for which the significant contribution to the Hamiltonian is indicated in Fig. 1(b). The importance of surface-charge discreteness has been known for decades [35,36]. For systems with dielectric interfaces, it can go much beyond the uniform surface-charge model in providing the correct prediction as the polarization charge modifies the binding energy of EDL ions [37]. In the model, the parameter ν is used to phenomenologically depict the strength of the short-range electrostatic correlation between the surface charges and counterions [38]. This parameter can either represent the valence of chemical groups on colloidal surfaces or represent the coarsened partial electronic charges localized on the NP. In electrochemical materials, the fluctuation of the charge distribution on the electrode screens the ion-ion interaction and it is reported to play an essential role predicting correct EDL capacitances [13–15,39]. Thus, the fluctuation surface-charge model with parameter ν is expected to mimic many physical systems that the uniform or fixed surface-charge models cannot reach.

In all simulations, the radius of the simulation cell takes $2.5R$, with radii of mobile ions $a_+ = 0.05R$, $a_- = 0.075R$ and the Bjerrum length $\ell_B = 0.5R$. The coion volume fraction of the Wigner-Seitz cell is fixed as $15.1(a_{coion}/R)^3$, while the number of counterions placed in the electrolyte is given by the electroneutrality constraint. We investigate both the HCP and LCP for different shell thickness $\theta = 0$–0.05 and correlation parameter $\nu = 0.1$–0.5. The size of the NP chosen in simulations is $R = 4$ nm, corresponding to a physical condition of bulk salt

concentration 100 mM and Debye length $\ell_D = 5.75$ Å in dimensional units.

To emphasize the important role of the shell, Fig. 2 shows normalized radial distribution functions (RDFs) of counterions for cases of the HCP and LCP with the fixed surface charge density and correlation strength for varying shell thicknesses. EDL structures of both cases are significantly different. For the HCP, the high-dielectric core provides an additional attraction to mobile ions; thus, the counterion density is very high without the shell layer, and decreases with the increase of the shell thickness due to the low-dielectric shell material. In the case of LCP, the core layer could lead to a depletion force to counterions, but due to the high-dielectric shell, which provides a local attraction to ions, the depletion zone vanishes with the increase of θ. The change in the magnitude of the RDF profile is decreasing as the increase of θ, and the structure of the EDL becomes less sensitive to the dielectric inhomogeneity if the shell is sufficiently thick.

One potentially important application of the core-shell NPs lies in the electrochemical capacitance, which can be viewed as a series combination of a quantum capacitance of the electrode and an EDL capacitance [40]. The quantum capacitance depends on the electron density of states in the electrode and can be described by the self-consistent relations between the electron density and the potential by electronic structure calculation, which is beyond the scope of this work. In a recent experiment, Ji *et al.* [41] studied layered electrodes with the graphene layers coated on the PMMA substrate, and observed that the EDL capacitance near the graphene electrode extremely depends on the number of graphene layers and the single-layer graphene maximizes the capacitance, and this abnormal enhancement is attributed to the correlation between electrode charges and electrolyte ions. We use the aforementioned core-shell NP system with the mobile surface-charge model with varying surface-charge strength ν, which represents both the integrated electronic charges [17] and the depth of them buried in the electrode. A larger ν then corresponds to smaller number of graphene layers. This simplification allows us with the first attempt to investigate the effect of core-shell structured dielectric inhomogeneity on the EDL capacitance through simulations. We measure the relative surface differential capacitance C/C_0 with $C = d\sigma/dV_s$, where V_s is the surface potential of the NP. C_0 is the capacitance obtained by the mean-field Gouy-Chapman-Stern theory in the linear regime, i.e., under the approximation of sufficient low V_s and $\sinh(\beta e V_s) \approx \beta e V_s$, with $\beta = 1/(k_B T)$:

$$C_0 = \frac{\varepsilon_w \varepsilon_0 [1 + \kappa(R + d)]}{R(1 + \kappa d)}. \qquad (9)$$

Here, κ is the inverse Debye length and $d = a_+$ is the Stern layer thickness. Capacitances for different θ but with fixed $\nu = 0.1$ versus surface potentials are presented in Figs. 3(a)
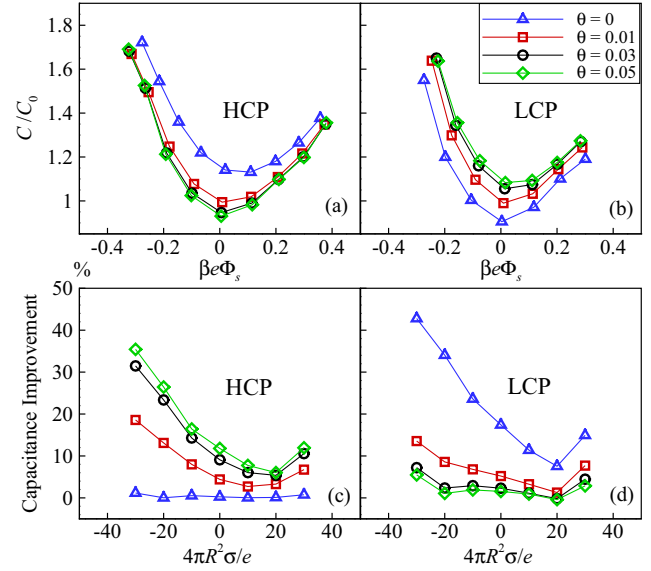
FIG. 3.   Scaled differential capacitances versus dimensionless surface potentials with different shell thicknesses $\theta = 0$–0.05 and a fixed correlation strength $\nu = 0.1$ are shown in (a) for the HCP and (b) for the LCP; the relative enhancements of differential capacitance from $\nu = 0.1$–0.5 versus dimensionless surface densities with different shell thicknesses $\theta = 0$–0.05 are shown in (c) for the HCP and (d) for the LCP.

and 3(b) to illustrate the results for the shell thickness θ from 0 to 0.05. It is observed that increasing θ leads to a decrease of capacitances for HCP [Fig. 3(a)] and an increase for LCP [Fig. 3(b)], respectively, indicating that dielectric boundary attractions enhance capacitances in agreement with the discussion in Ref. [39], and high-ε materials usually lead to high energy storage capabilities.

The effect of the ion-interface correlation strength on the capacitance is also investigated by tuning the parameter ν from 0.1 to 0.5. A larger ν corresponds to stronger correlations between surface charges and counterions, which leads to tighter binding of counterions to the surface, narrowing the electric double layer and generally increasing the capacitance. Figures 3(c) and 3(d) show the calculation of the enhancement percentage of capacitances defined as $(C^{\nu=0.5} - C^{\nu=0.1})/C^{\nu=0.1}$. For the HCP [Fig. 3(c)], the capacitance improvement turns out to be more obvious for larger θ since the interaction energy between an ion and a surface charge becomes larger [Fig. 1(b)]. In contrast, for a LCP [Fig. 3(d)], the maximal capacitance improvement happens at $\theta = 0$ when the ion-interfacial charge interaction is maximum. In both cases, we can draw the conclusion that stronger mobile ion-interfacial charge correlations do lead to more significant capacitance improvements. This is in agreement with experimental observations for electrodes with layered materials [41].

In summary, we have developed a general ICM, enabling accurate and efficient simulations for a dielectric core-shell structured NP immersed in an electrolyte. We incorporate

our method into MC simulations and explore the core-shell structured dielectric boundary effects on EDL structures and capacitances, which, in general, show that dielectric boundary attractions and strong correlations between mobile ions and interfacial charges enhance EDL capacitances. It is also demonstrated that these phenomena can be well explained by our analysis on self-energy and interaction energy profiles. The approach can be generalized to (a) systems with multilayers or dielectric functions if the Poisson's equation can be solved with spherical harmonic expansions and (b) systems with multiple core-shell NPs by incorporation with the hybrid method of images and moments [22]. Both cases will be the topic of our future studies. Finally, based on this work, it is now possible to quantitatively study dielectric effects for dielectrically inhomogeneous NPs, which may help shed light on the mechanisms of existing experimental observations and direct the design of energy storage devices made of core-shell structured NPs.

[*]mmm@sjtu.edu.cn
[†]Current address: Department of of Mathematics, University of Michigan, Ann Arbor, MI 48109, USA.
[‡]xuzl@sjtu.edu.cn

[1] K. Chatterjee, S. Sarkar, K. J. Rao, and S. Paria, Adv. Colloid Interface Sci. **209**, 8 (2014).
[2] J. Li, L. Zhang, and S. Ducharme, Appl. Phys. Lett. **90**, 132901 (2007).
[3] X. Huang and P. Jiang, Adv. Mater. **27**, 546 (2015).
[4] Y. Lu and M. Ballauff, Prog. Polym. Sci. **36**, 767 (2011).
[5] K. Yang, X. Huang, M. Zhu, L. Xie, T. Tanaka, and P. Jiang, ACS Appl. Mater. Interfaces **6**, 1812 (2014).
[6] R. Contreras-Cáceres, A. Sánchez-Iglesias, M. Karg, I. Pastoriza-Santos, J. Pérez-Juste, J. Pacifico, T. Hellweg, A. Fernández-Barbero, and L. M. Liz-Marzán, Adv. Mater. **20**, 1666 (2008).
[7] Y. Min, M. Akbulut, K. Kristiansen, Y. Golan, and J. Israelachvili, Nat. Mater. **7**, 527 (2008).
[8] Y. Zhou, Z.-Y. Qin, L. Li, Y. Zhang, Y.-L. Wei, L.-F. Wang, and M.-F. Zhu, Electrochim. Acta **55**, 3904 (2010).
[9] L. Bao, J. Zang, and X. Li, Nano Lett. **11**, 1215 (2011).
[10] X. Xia, J. Tu, Y. Zhang, X. Wang, C. Gu, X.-B. Zhao, and H. J. Fan, ACS Nano **6**, 5531 (2012).
[11] J. W. Zwanikken and M. O. de la Cruz, Proc. Natl. Acad. Sci. U.S.A. **110**, 5301 (2013).
[12] K. Barros and E. Luijten, Phys. Rev. Lett. **113**, 017801 (2014).
[13] M. S. Loth, B. Skinner, and B. I. Shklovskii, Phys. Rev. E **82**, 056102 (2010).
[14] B. Skinner, T. Chen, M. S. Loth, and B. I. Shklovskii, Phys. Rev. E **83**, 056102 (2011).
[15] S. Kondrat and A. Kornyshev, J. Phys. Condens. Matter **23**, 022201 (2011).
[16] D. T. Limmer, C. Merlet, M. Salanne, D. Chandler, P. A. Madden, R. van Roij, and B. Rotenberg, Phys. Rev. Lett. **111**, 106102 (2013).
[17] C. Merlet, B. Rotenberg, P. A. Madden, and M. Salanne, Phys. Chem. Chem. Phys. **15**, 15781 (2013).
[18] R. Wang and Z.-G. Wang, J. Chem. Phys. **139**, 124702 (2013).
[19] Y. S. Jho, M. Kanduc, A. Naji, R. Podgornik, M. W. Kim, and P. A. Pincus, Phys. Rev. Lett. **101**, 188101 (2008).
[20] B. Chu, X. Zhou, K. Ren, B. Neese, M. Lin, Q. Wang, F. Bauer, and Q. Zhang, Science **313**, 334 (2006).
[21] I. V. Lindell, M. E. Ermutlu, and A. H. Sihvola, IEE Proc. H, Microw. Antennas Propag. **139**, 186 (1992).
[22] Z. Gan, S. Jiang, E. Luijten, and Z. Xu, SIAM J. Sci. Comput. **38**, B375 (2016).
[23] V. Jadhao, F. J. Solis, and M. O. de la Cruz, Phys. Rev. Lett. **109**, 223905 (2012).
[24] F. Fahrenberger, O. A. Hickey, J. Smiatek, and C. Holm, Phys. Rev. Lett. **115**, 118301 (2015).
[25] A. C. Maggs and V. Rossetto, Phys. Rev. Lett. **88**, 196402 (2002).
[26] See Supplemental Material at http://link.aps.org/supplemental/10.1103/PhysRevLett.118.076102, which includes Ref. [27], for detailed descriptions of the asymptotic analysis and numerical efficiency.
[27] I. S. Gradshteyn and I. M. Ryzhik, *Table of Integrals, Series and Products*, 7th ed. (Academic Press, San Diego, 2007).
[28] J. D. Jackson, *Classical Electrodynamics*, 3rd ed. (John Wiley & Sons, New York, 2001).
[29] C. Neumann, *Hydrodynamische Untersuchungen: nebst einem Anhange uber die Probleme der elektrostatik und der magnetischen Induktion* (Teubner, Leipzig, 1883), pp. 279–282.
[30] I. V. Lindell, Radio Sci. **27**, 1 (1992).
[31] W. Cai, S. Deng, and D. Jacobs, J. Comput. Phys. **223**, 846 (2007).
[32] Z. Xu, Y. Liang, and X. Xing, SIAM J. Appl. Math. **73**, 1396 (2013).
[33] P. Linse, Adv. Polym. Sci. **185**, 111 (2005).
[34] K. Qamhieh and P. Linse, J. Chem. Phys. **123**, 104901 (2005).
[35] S. Levine, G. M. Bell, and D. Calvert, Can. J. Chem. **40**, 518 (1962).
[36] R. Brown, Prog. Biophys. Molec. Biol. **28**, 341 (1974).
[37] Z. Gan, X. Xing, and Z. Xu, J. Chem. Phys. **137**, 034708 (2012).
[38] B. I. Shklovskii, Phys. Rev. Lett. **82**, 3268 (1999).
[39] B. Skinner, M. S. Loth, and B. I. Shklovskii, Phys. Rev. Lett. **104**, 128302 (2010).
[40] S. Datta, *Quantum Transport: Atom to Transistor* (Cambridge University Press, Cambridge, 2005).
[41] H. Ji, X. Zhao, Z. Qiao, J. Jung, Y. Zhu, Y. Lu, L. L. Zhang, A. H. MacDonald, and R. S. Ruoff, Nat. Commun. **5**, 3317 (2014).